Pigment-Macromolecule Complexes Isolation from Sea Urchin Biomineral Waste for Coloring Materials

Claudio Ferreira, Vaskar Sardhalia, Alshaba Kakar, Romain Descamps, Lucrèce Matheron, François Ribot, Alexandre Disser, Tony Jouanneau, Elena Vasileva, Natalia Mishchenko, et al.

Pigment-Macromolecule Complexes Isolation from Sea Urchin Biomineral Waste for Coloring Materials

Claudio Ferreira, Vaskar Sardhalia, Alshaba Kakar, Romain Descamps, Lucrèce Matheron, François Ribot, Alexandre Disser, Tony Jouanneau, Elena Vasileva, Natalia Mishchenko, Nadine Nassif, Frédéric Marin, and Marie Albéric*

The production and widespread use of synthetic pigments and dyes have significant environmental and health impacts. Despite this, synthetic colorants remain dominant due to their wide color range, high stability, strong tinting power, and lower cost compared to natural alternatives. Therefore, to offer sustainable and competitive substitutes, eco-friendly methods for producing bio-based pigments with similar performance are essential. Herein, a methodology has been developed to extract the entire colored organic fraction occluded within seashell biomineral waste, which comprises pigments and pigment-macromolecule complexes. This process involves an optimized cleaning procedure of the biomineral soft tissues, a tailored biochemical extraction, and detailed characterization of the extracted fraction. Applied to sea urchin skeletons, this method successfully isolates polyhydroxylated naphthoquinone (PHNQ)-macromolecule complexes. These complexes show superior pH stability in purple hues compared to free PHNQ, which shifts from red to purple in basic conditions. Notably, the approach enhances colorant yield by up to five times. These results, together with mineral pigment synthesis and fabric dyeing assays performed with the extracted colored organic fraction, contribute to a better understanding of the origin of color in biominerals and reveal the versatility of these natural pigments for environmentally friendly coloring of both organic and inorganic materials.

1. Introduction

For thousands of years, organic pigments have been extracted from biological materials (e.g., murex, cochineal, cuttlefish, plants such as indigo, madder, walnut, and henna) for various uses, including dyes, inks, paints, and medicines.[1] By the 19th century, natural colorants had largely been replaced by synthetic ones because these are more stable, cheaper, and offer a broader

C. Ferreira, V. Sardhalia, A. Kakar, F. Ribot, N. Nassif, M. Albéric
Laboratoire de Chimie de la Matière Condensée de Paris (LCMCP)
Sorbonne Université
CNRS
75005 Paris, France
E-mail: marie.alberic@sorbonne-universite.fr

R. Descamps
Plateforme de Chimie Analytique
Physique et Spectroscopie
Sorbonne Université
75005 Paris, France

L. Matheron
Institut de Biologie Paris Seine
CNRS
Sorbonne Université
75005 Paris, France

L. Matheron
Fédération de Chimie Moléculaire Paris Centre
CNRS
Plateforme MS^{3}U
Sorbonne Université
75005 Paris, France

A. Disser
LAPA-IRAMAT UMR 7065 & LAPA-NIMBE UMR 3685
CNRS
CEA
Université Paris-Saclay
91191 Gif-sur-Yvette, France

T. Jouanneau
Jardin des métiers d'Art et du Design
Atelier SUMBIOSIS
92310 Sèvres, France

E. Vasileva, N. Mishchenko
Laboratory of the Chemistry of Natural Quinonoid Compounds
G.B. Elyakov Pacific Institute of Bioorganic Chemistry
Far Eastern Branch of Russian Academy of Sciences
Vladivostok 690022, Russia

F. Marin
Laboratoire Biogéosciences
UMR CNRS-EPHE-UBE 6282
Université Bourgogne Europe (UBE)
21000 Dijon, France

Supporting information for this article is available on the WWW under https://doi.org/10.1002/cmtd.202500078

range of colors.[2] However, their production, based on petrochemicals, as well as their use, has a significant impact on the environment and human health, especially in the textile industry, which is one of the most polluting industries globally.[3] Therefore, replacing synthetic colorants with bio-based ones that have competitive properties is now a top priority for various industries, including coatings, paints, textiles, food, cosmetics, and construction.

A promising—yet poorly investigated—source of natural pigments is the small organic molecules (<1 kDa) (e.g., polyenes, porphyrins, bilins, melanins, and quinonoids such as anthraquinones, polycyclic quinones, naphthoquinones) incorporated within calcium carbonate ($CaCO_3$)-based biominerals of crustaceans, mollusks, and echinoderms.[4,5] Indeed, these pigments provide these biominerals a wide range of stable color nuances from yellow, red, purple, and green, and can be recycled from seashell waste that accounts for over 18 million tons every year.[6–8] In the case of sea urchins, polyhydroxylated-naphthoquinone pigments (PHNQs), particularly the so-called echinochrome A molecule ($C_{12}H_{10}O_7$, 7-ethyl-2,3,5,6,8-pentahydroxy-1,4-naphthoquinone) already utilized for pharmaceutical applications,[9–11] exhibit demonstrated antimicrobial, anti-inflammatory, antioxidant, and UV-absorption properties.[12–16] Synthesized by sea urchins through enzymatic pathways, PHNQs are secondary metabolites occluded within the $CaCO_3$ mineral phase most likely during its growth,[17,18] i.e., biomineralization processes. Other organic molecules, such as proteins, glycoproteins, and polysaccharides known to be involved in biomineralization mechanisms, are also encapsulated within the mineral phase[19] and may thus interact with PHNQs.

Stable in acidic conditions,[20] PHNQs have been previously extracted through the dissolution of the mineral phase using strong acids (such as HCl), acidified ethanol (4–10% H_2SO_4), or formic acid (6 M).[11,16,20–23] Such conditions allow for the isolation and purification of free pigment molecules, but not for recovering proteins and polysaccharides, which are either destroyed or insoluble in the solvent considered. Instead, such macromolecules are classically extracted in aqueous solution under mild dissolution conditions using, e.g., diluted acetic acid,[24,25] and further separated, concentrated, and purified using ultrafiltration and dialysis steps with a cut-off above 1 kDa,[25–29] thereby precluding the isolation of smaller pigment molecules, such as PHNQs (approximately 250 Da). Since pigments and macromolecules are expected to form complexes within the mineral phase,[30–33] their simultaneous extraction is therefore essential for studying pigmentation mechanisms during biomineralization and for further investigating their peculiar color properties in terms of hues, tinting strength, and stability. We also hypothesize that these biological intrinsic color properties are interesting for proposing natural colorants competitive with synthetic dyes.

As a result, we here present a methodology developed for the isolation and characterization of both small pigment molecules and macromolecules occluded within colored biomineral waste (**Figure 1**). This developed methodology includes 1) an optimized cleaning procedure of the biominerals, 2) a customized biochemical extraction protocol, and 3) a thorough characterization of the

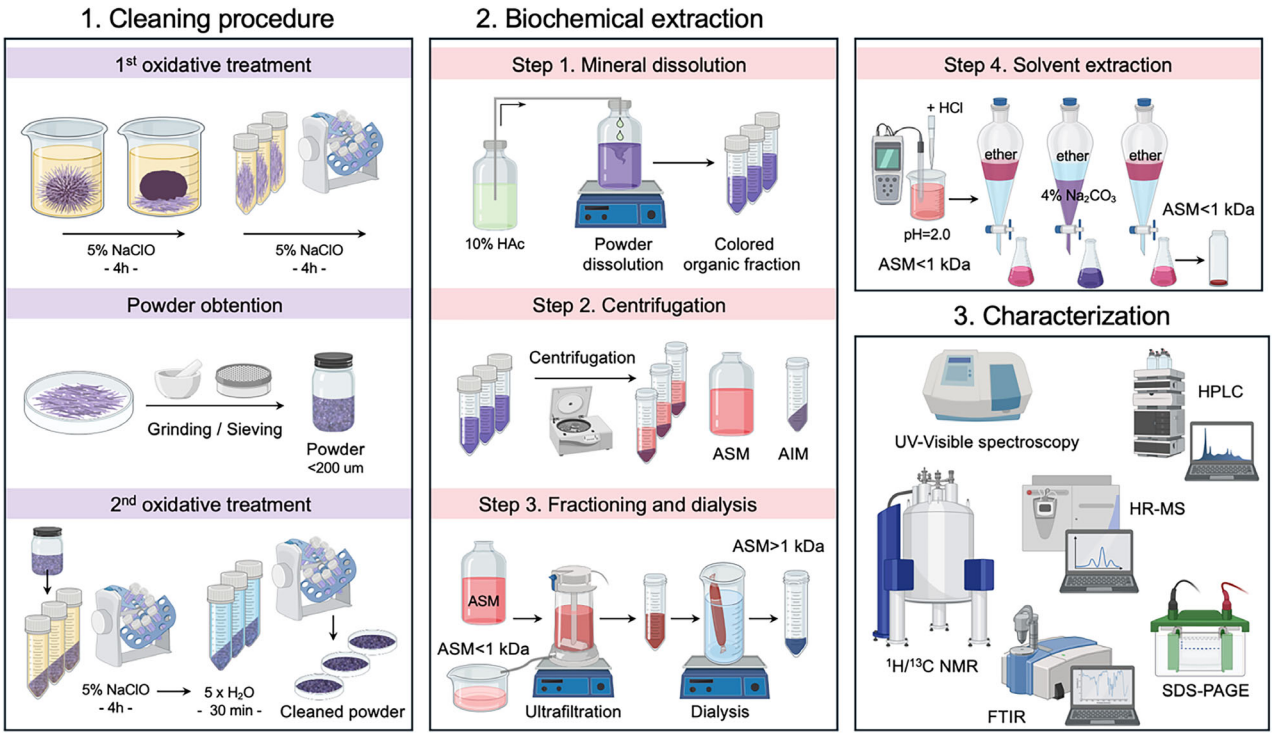

Figure 1. Scheme of the developed methodology for the isolation and characterization of the intracrystalline colored organic fraction of biominerals including 1) the cleaning procedure, 2) the biochemical extraction protocol, and 3) the different analytical techniques considered. %NaClO: wt% of active chlorine of NaClO, HAc: acetic acid, AIM: acid insoluble matrix, ASM: acid soluble matrix.

colored organic fraction by High-Performance Liquid Chromatography-Mass Spectrometry (HPLC-MS), ^{1}H and ^{13}C Nuclear magnetic resonance (NMR), high-resolution (HR)-MS, UV–visible spectroscopy, and SDS-polyacrylamide gel electrophoresis (PAGE). This methodology is applied here to purple sea urchin spines from the edible *Paracentrotus lividus* species, but can be extended to other species that present an intracrystalline colored organic fraction. Our results validate the occurrence of PHNQ-macromolecule complexes within the mass-colored $CaCO_3$-biominerals, in addition to free PHNQs. Notably, isolated PHNQ-macromolecule complexes exhibit a stable purple color in solution, regardless of pH, in contrast to free PHNQs, which change from red to purple at basic pH. Finally, we show the interest of the present methodology by performing bio-inspired synthesis of calcium carbonate in the presence of the extracted colored organic fraction and by successfully dyeing silk and wool fabrics.

2. Results and Discussion

2.1. Quantification of the Color and Removal of the Connective Tissues Surrounding the Biominerals

Biominerals are usually closely associated with soft connective tissues during the lifetime of organisms. In particular, *Paracentrotus lividus* sea urchin spines are covered by an epithelium that, once removed by 5% NaClO soaking for 4h, reveals the purple color of the biominerals (**Figure 2**A–C). This observation confirms that the purple hue originates from pigment molecules occluded within the biominerals, rather than those present in the soft tissues. To further evaluate the color spreading within the mineralized structure, polished cross-sections of the spines were obtained after resin embedding (Figure 2D-F). Light microscopy observations of the cross-sections reveal that the purple color is evenly distributed throughout the biominerals. Indeed, the radial dense wedges (called septa) display an intense purple color homogeneously distributed at the microscale (Figure 2E). At the same time, the porous inner structure (named stereom) shows a heterogeneously distributed purple hue (Figure 2F), possibly due to different concentrations of pigment molecules and/or lower mineral thicknesses in this region. The observed mass-coloration indicates that pigment molecules are continuously deposited and encapsulated during the two main growth events of the spines, i.e., stereom and septa formation.[34,35] Sea urchins, therefore, appear to effectively concentrate colored molecules in their spines, making them an interesting resource for pigment extraction with a promising yield.

Before extracting the organic fraction occluded within the mineral phase (termed intracrystalline organics), the soft tissues must be removed to avoid any contamination of the final extracts. In earlier works, soft tissues were removed by collagenase,[36] NH_4OH,[37] H_2O_2,[38] or NaClO bleaching treatments.[38–42] Typically, two oxidative treatments are performed to ensure the complete removal of soft tissues tightly bound to the biomineral surface: first on the entire biomineral and second on powdered samples.[38–40,43] After performing the first oxidative treatment of the whole spines for 8h with 5% NaClO (Figure 1), some soft tissues are indeed still observed, in particular at the surface of the convoluted stereom pores (**Figure 3**A). Previously, a second treatment of 12% NaClO for 48h was shown to be the most efficient for completely removing the intercrystalline (non-occluded) organics from mollusk shell powders.[38] This second treatment is also considered for sea urchin spines and indeed shows an efficient removal of the soft tissues within the convoluted stereom pores (Figure 3B). However, fractured spine sections treated in these alkaline conditions (pH = 11) show significant etching of their surfaces (Figure 3B, white stars) compared to unbleached fractured spines, which display typical conchoidal fractures

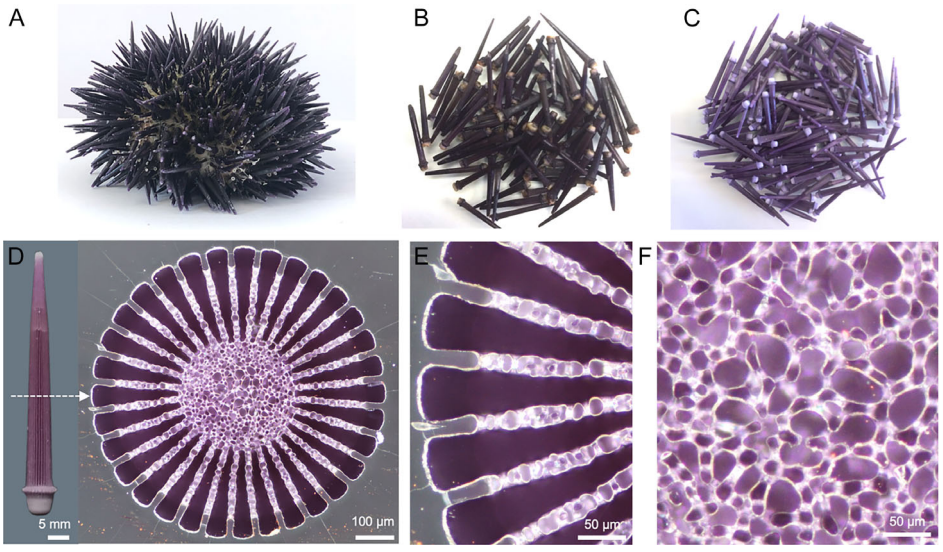

Figure 2. A) Sea urchin *Paracentrotus lividus* after dissection, B) spines with connective tissues after manual removal from the test, C) spines after removal of connective tissues with 5% NaClO, D) optical images of a spine cross-section after resin embedding, E) magnification of the septa and F) magnification of the stereom.

(Figure 3A, white arrows). The bleached surfaces present rough, wavy patterns in the septa and concentric layers in the stereom. These patterns resemble the ones classically observed when acidic solutions or calcium-chelating agents (such as EDTA) are used to partially dissolve the calcite phase and expose the intracrystalline organics.[18,26,44] Here, intracrystalline organics are, in contrast, probably removed from the surface of the fractured sections, leaving a negative pattern comparable to the concentric layers previously evidenced by the effect of digestive enzymes on fractured sea star spines.[45] This second oxidative treatment is therefore too drastic in the case of sea urchin spines, as it induces some loss of the intracrystalline organics.

To minimize such loss, which would be even higher for powdered spines, cleaning conditions with lower NaClO concentrations (4-6% or 1-2%) were tested for 48h, 24h, 12h, and 4h (Figure 3C and Figure S1, Supporting Information). Interestingly, the results show that the degree of etching decreases with shorter exposure times, but not necessarily with lower concentrations, and that a treatment of 4 h with 5% NaClO limits the loss of intracrystalline organics while still ensuring efficient removal of the soft tissues.

After optimizing the cleaning procedure, the colors of the powdered biominerals are quantified before and after the second bleaching treatment to ensure the preservation of the intracrystalline, colored organic fraction. This quantification is performed using UV–visible diffuse reflectance spectroscopy (DRS) measurements, which allow for the determination of the L*, a*, b* parameters, as well as the RGB values (see Experimental Section). The spectrum of the purple spine powder (<200 µm) after the first NaClO treatment displays three intense UV bands at 245, 295, and 355 nm as well as two bands in the visible range: a small one at 480 nm and a more intense and broader one at 570 nm (**Figure 4**A). The UV bands are typical of aromatic and quinonoid charge transfers of naphthoquinones, and the visible bands, responsible for the purple color, correlate with the red shift of quinonoid electronic transitions due to the presence of hydroxyl substituents.[20,46,47] For this sample, $L^* = 69.9$, $a^* = 6.79$, $b^* = -8.5$, and the RGB values are 178, 167, and 187. After the second NaClO treatment, similar UV–visible bands are measured, therefore indicating the preservation of the molecular structure of PHNQs and of the color as confirmed by similar L*, a*, b*, and RGB values (L*: 68.3, a*: 7.3, b*: −8.8, R: 174, G: 162, B: 183) and the

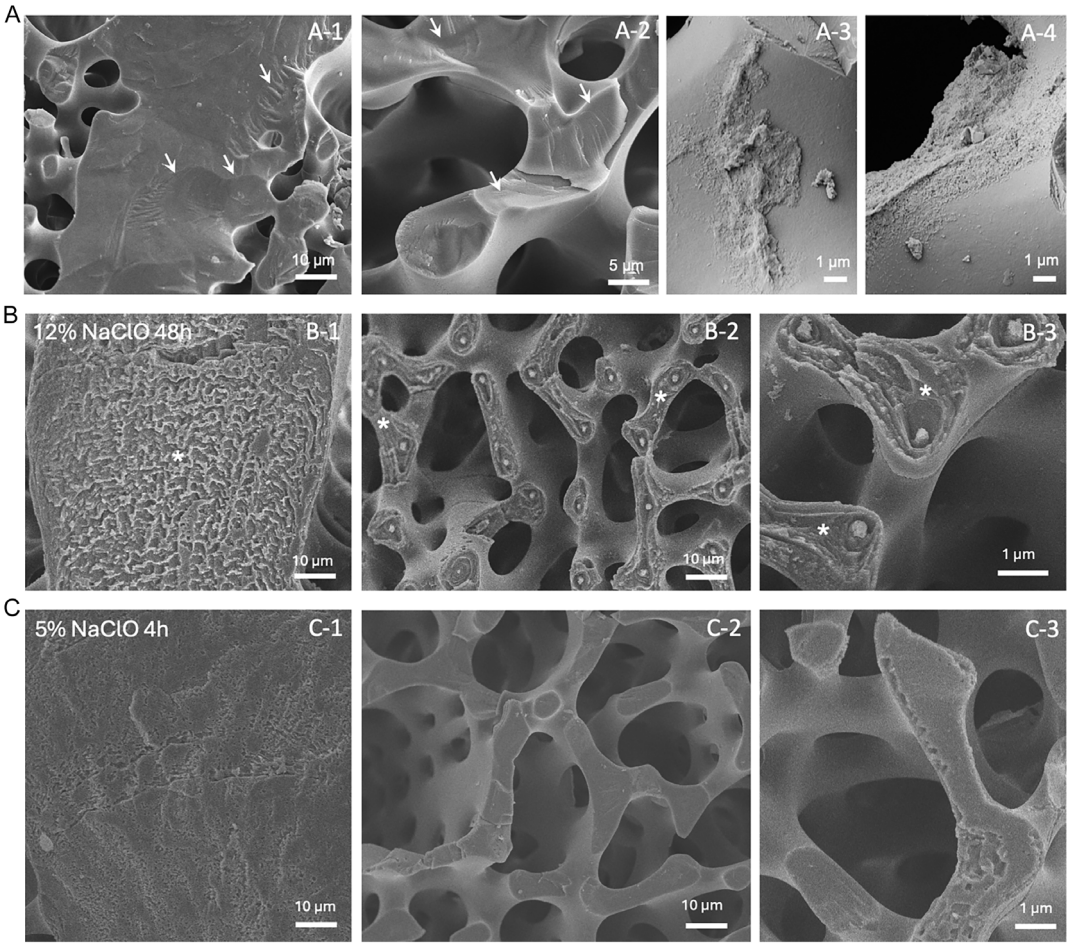

Figure 3. SEM micrographs of fractured spines cleaned with A) the first treatment only, A-1 area one septum, A-2-4 areas in the stereom; and with the second oxidation NaClO treatment B) with 12% NaClO cleaning for 48 h, B-1 area in one septum, B-2-3 areas in the stereom; and C) 5% NaClO for 4 h, C-1 area in one septum, C-2-3 areas in the stereom.% NaClO: wt% of active chlorine of NaClO. White arrows show the conchoidal fracture of the spines and the white stars indicate the etching.

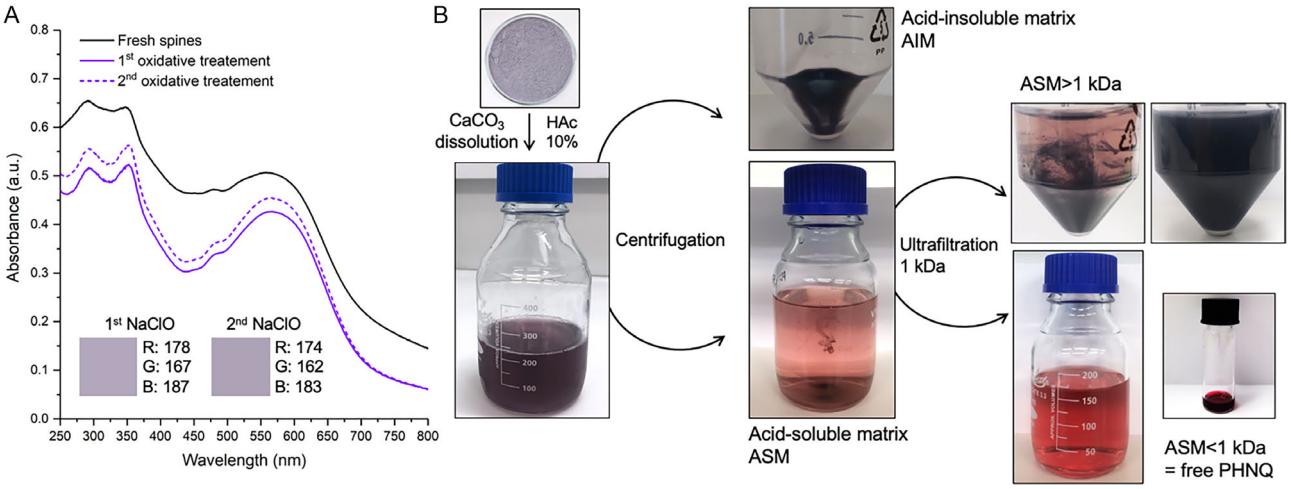

Figure 4. A) UV–visible DRS spectra of spine powder before and after second oxidative treatment with 4% NaClO for 12h, B) photographs of the extracts collected at the different key steps of the extraction protocol: after mineral dissolution, centrifugation and ultrafiltration. %NaClO: wt% of active chlorine of NaClO.

calculation of a low deltaE CIE 2000 of 1.4.[48] This result confirms the occlusion of the pigment molecules within the biomineral and their subsequent protection from oxidative treatment. Similarly to the well-studied intracrystalline macromolecules of biominerals,[18,49–52] PHNQs are therefore also considered intracrystalline organic molecules. We note that when occluded, PHNQs maintain their characteristic UV-absorption properties, thus supporting one of the hypotheses regarding their physiological function as UV-protectants.[12]

2.2. Extraction and Purification of the Intracrystalline Colored Organic Fraction

After applying the optimized cleaning procedure of the biominerals (1), the customized biochemical extraction protocol (2) is performed to isolate the entire intracrystalline colored organic fraction that is subsequently separated and purified into three different subfractions detailed below. The three fractions are finally thoroughly characterized (3) by HPLC-MS, ^{1}H and ^{13}C NMR, HR-MS, UV–visible spectroscopy, and SDS-PAGE (Figure 1).

The first step of the extraction protocol involves a complete mineral dissolution under mild conditions, i.e., using diluted acetic acid (10 vol.%, pH 2.5) to preserve macromolecules that may be associated with pigments, which strong acids would otherwise destroy.[22,53] EDTA can also be used for decalcification,[33,37,54] but since it tends to form complexes with macromolecules, its further removal is quite challenging.[55,56] After complete mineral dissolution of the purple powder ($<$200 µm), a purple solution (pH 4.4) is obtained. The second step involves separating the purple solution by centrifugation into two fractions: a solid pellet consisting of the acid-insoluble matrix (AIM) fraction and the supernatant containing the acid-soluble matrix (ASM) fraction. The AIM displays a dark purple color while the supernatant is pinkish in color and presents a dark purple colloidal suspension (Figure 4B). These different colors indicate different pigment compositions, concentrations, ionic forms, and/or association with macromolecules.

The third step involves separating the ASM solution by size using ultrafiltration with a 1 kDa cut-off membrane and purifying it. The separation allows for isolating the pigment molecules associated with macromolecules (ASM $>$ 1 kDa) from the free pigment molecules (ASM $<$ 1 kDa), which are approximately 250 Da for PHNQs. In contrast to previous studies,[25–29] the ASM $<$ 1 kDa fraction is recovered for further purification and structure elucidation of the pigment molecules. In the case of purple spines, ASM $<$ 1 kDa displays an intense and translucent pink color, whereas ASM $>$ 1 kDa is opaque and shows a biphasic coloration due to the presence of the highly concentrated dark colloidal suspension mentioned above (Figure 4B). The purification of the ASM $>$ 1 kDa fraction (*i.e.*, removal of acetic acid and dissolved salts) is typically performed by extensive dialysis against distilled water, using dialysis membrane tubes with a 1 kDa cut-off.

The fourth step is the purification of the ASM fraction $<$ 1 kDa, mainly composed of PHNQs, by solvent extraction using diethyl ether[22] or ethyl acetate.[11] To optimize the detection of PHNQs by ^{1}H NMR, this fraction must be further purified from remaining small lipids by Na_2CO_3 treatment[57] and then freeze-dried to minimize the amount of water. Once concentrated with diethyl ether, ASM $<$ 1 kDa displays an intense ruby color, in agreement with a previous report[22] (Figure 4B).

The other fractions are also freeze-dried and weighed. The yield of the AIM + ASM $>$ 1 kDa fractions varies from 0.1 to 0.5 wt% while the one of the ASM $<$ 1 kDa fraction, i.e., the free PHNQs, is from 0.05 to 0.15 wt%. The latter is in agreement with previously reported yields for free PHNQ extracts from the *P. lividus* species[23,58] and is comparable to that from the *Scaphechinus mirabilis* species, which is used for the extraction of Echinochrome A and is already commercialized for medicinal purposes.[11] Therefore, the extraction of the complete colored organic fraction presents a first advantage, namely, increasing

the colorant extraction yield up to fivefold. The developed protocol thus provides an interesting strategy for valorizing edible sea urchin waste to obtain natural dyes that also possess potential antibacterial, antioxidant, and UV-protectant properties, while being environmentally friendly.

2.3. Structure Elucidation of the Small Pigment Molecules

Among the large number of PHNQ molecules previously identified in various sea urchin species,[11] five PHNQs have been reported for *P. lividus* based on UV–visible spectroscopy, ultrahigh-performance liquid chromatography (UPLC) and UPLC-HR-MS, namely, echinochrome A ($C_{12}H_{10}O_7$, 7-Ethyl-2,3,5,6,8-pentahydroxy-1,4-naphthoquinone), spinochrome A ($C_{12}O_7H_8$, 3-Acetyl-2,5,7,8-tetrahydoxy-1,4-naphthoquinone), spinochrome B ($C_{10}O_6H_6$, 2,3,5,7-Tetrahydroxy-1,4-naphthoquinone), spinochrome C ($C_{12}O_8H_8$, 2-Acetyl-3,5,6,7,8-pentahydroxy-1,4-naphthoquinone), and spinochrome E ($C_{10}H_6O_8$, 2,3,5,6,7,8-Hexahydroxy-1,4-naphthoquinone).[10,22,23,58–60]

Here, the ASM $<$ 1 kDa is first analyzed by 2D ^{1}H-^{13}C heteronuclear multiple bond correlation (HMBC) NMR spectroscopy (**Figure 5**A). The ^{1}H and ^{13}C signal assignments, along with the HMBC correlations, are summarized in Table S1, Supporting Information. The chemical shifts for all ^{1}H ($H_a - H_f$) and for eight of the twelve ^{13}C (C3, C5 – C11) could be measured. HMBC cross-peaks for H_d are not observed due to the low signal intensity of β-hydroxyl in spinochromes, as reported previously.[9,11] All the ^{1}H and ^{13}C assignments, as well as the observed correlations, are in line with the structure of spinochrome A. This is the first HMBC experiment reported for spinochrome A in the literature, to our knowledge, and is consistent with trends in chemical shifts for similar molecules.[9,61] These results show that spinochrome A is the main free PHNQ of the ASM $<$ 1 kDa fraction. Small ^{1}H peaks tagged as (*) are too low in intensity to be evaluated and may correspond to other PHNQs present in lower concentrations.

Consequently, HPLC-MS and HR-MS analyses were further performed to assess the nature of these minor molecules. The HPLC chromatogram shows two intense, defined elution peaks at 19.1 and 26.2 min (Figure S2A, Supporting Information), which are likely related to the mass detected at 19.3 min corresponding to spinochrome A (m/z 263) and the one measured at 26.3 min attributed to echinochrome A (m/z 265) (Figure S2B, Supporting Information). A smaller peak is also detected at 13.7 min in the chromatogram, corresponding to the mass detected at 13.9 min, which is attributed to spinochrome B (m/z 221). These results indicate the minor presence of echinochrome A and spinochrome B and confirm the major presence of spinochrome A.

HR-MS analyses with a nominal resolution of 30,000, which results in measured m/z accuracy $<$ 2 ppm, further allow for validating the presence of specific PHNQs based on the experimental mass once compared to the theoretical one. Experimental data reveal an intense peak at m/z 263.0196 (second isotope at 264.0229, see Experimental Section) and small peaks at

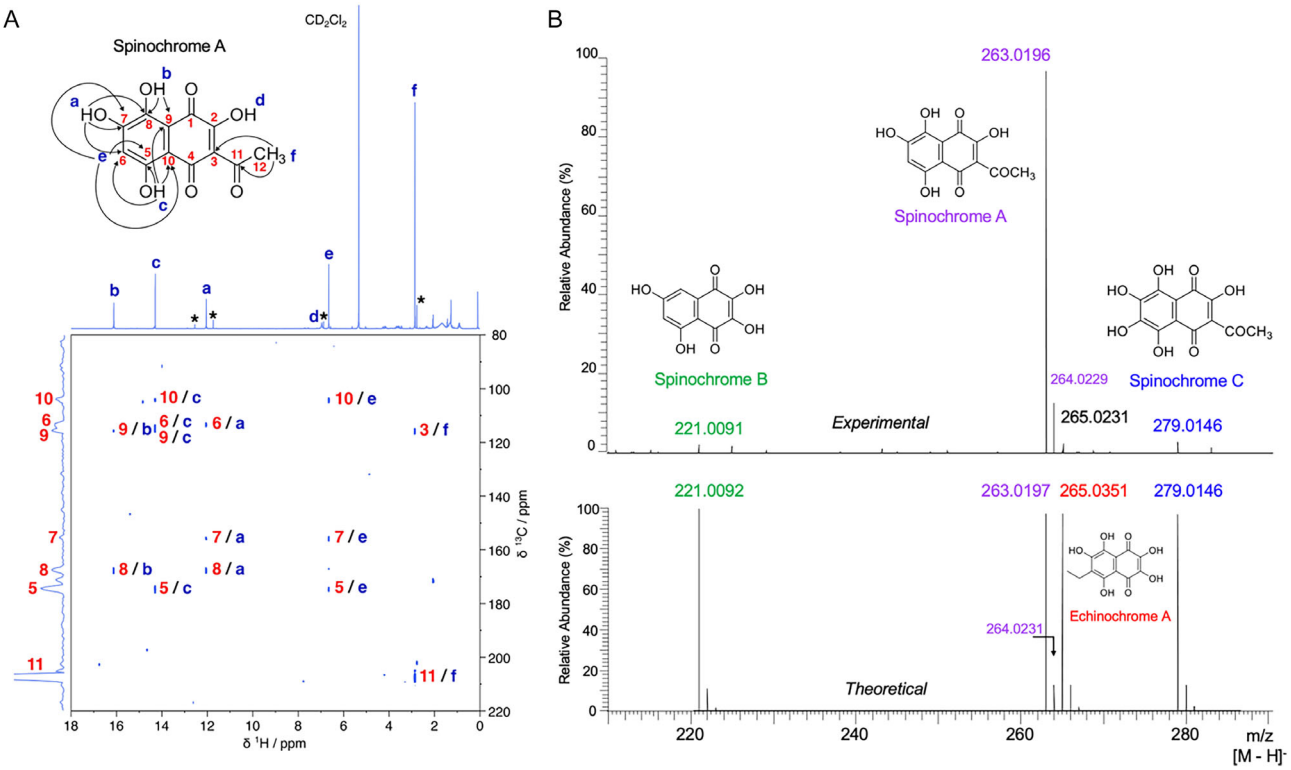

Figure 5. A) 2D ^{1}H and ^{13}C NMR spectroscopy through heteronuclear multiple bond coherence of ASM $<$ 1 kDa and B) HR-MS results of the same fraction showing the experimental mass m z^{-1} (top) and the theoretical one (bottom) of spinochrome B, spinochrome A, echinochrome A, and spinochrome C.

221.0091, 265.0230, and 279.0144 (Figure 5B). The presence of spinochrome A with a theoretical mass of 263.0198, that of spinochrome B with 221.0092, and that of spinochrome C with 279.0146 is thus confirmed. The theoretical mass for echinochrome A of 265.0351, however, indicates that it is in fact absent in this extract, although HPLC-MS with low-resolution MS seemed to indicate its presence. Indeed, the species detected at m/z 265.0230 would result in a mass error of −45.7 ppm if attributed to echinochrome A, which is too high for HR-MS. It might instead indicate the presence of PHNQ degradation products[62] or an unknown PHNQ, based on the predicted mass defect, which is the difference between the mass measured with HR-MS and the nominal mass. Indeed, the mass defect is relatively small (0.0230), suggesting that this molecule is rich in O atoms (atomic mass 15.9949 u for the most abundant isotope) compared to typical organic molecules composed mostly of C (12.0000 u) and H (1.0078 u) with higher mass defects.

Thus, this combination of analytical techniques confirms the predominant presence of spinochrome A and the minor occurrence of spinochrome B and C in the free pigment fraction (ASM $<$ 1 kDa).

2.4. Characterization of the Colored Macromolecule Fractions

The intense colors of the AIM and ASM $>$ 1 kDa fractions suggest the presence of the PHNQ pigments, which are probably bound to macromolecules, including proteins previously identified in sea urchin biominerals.[63,64] This possible association is first studied during the extraction protocol, i.e., in acetic acid (at pH 4.4) by UV–visible measurements for the soluble ASM $>$ 1 kDa fraction and the free PHNQ fraction composed mainly of spinochrome A. In agreement with previous reports,[11,22] the UV–visible spectrum of spinochrome A shows two defined UV bands at 273 and 311 nm and a broad visible band with absorption maximum at 510 nm (**Figure 6**A). Similarly to the purple spine powder (Figure 4A), the UV bands are here attributed to the aromatic and quinonoid charge transfers of naphthoquinones, while the visible band to the red color of this fraction. After homogenization, the ASM $>$ 1 kDa fraction shows a similar spectrum to that of free spinochrome A, with a redshift to 650 nm, which correlates with the observed dark navy color. The presence of the characteristic bands of spinochrome A in the ASM $>$ 1 kDa confirms its association with some macromolecules. After sedimentation of the dark colloidal suspension, the supernatant shows the same bands as those of free spinochrome A. This suggests the presence of spinochrome A in its free form versus complexed in the dark suspension. Note that a band is also detected at around 675 nm, attributed to the minor presence of the complexed form.

To confirm the nature of the PHNQs associated with the ASM $>$ 1 kDa fraction and determine that of the AIM, HR-MS analyses were performed after HCl acidification allowing for the removal of the macromolecules and further solvent extraction for isolating the potential PHNQs. The resulting mass spectra of both fractions show the presence of spinochrome A (Figure S3A-B,Supporting Information main peak at m/z 263.0196 and 263.0197). Very small peaks are attributed to the additional presence of spinochrome B in both fractions, as well as spinochrome C in ASM $<$ 1 kDa and echinochrome A in AIM. These results confirm that spinochrome A is the main PHNQ molecule associated with the macromolecules of both fractions.

The characterization of the different macromolecules associated with spinochrome A is typically performed through Fourier transform infrared (FTIR) analysis, which enables the screening of lipids, polysaccharides, and proteins. The FTIR spectra of the AIM and ASM $>$ 1 kDa fractions show indeed characteristic vibration bands of protein backbone and polysaccharide moieties (Figure 6B). Regarding the polysaccharide signatures, O—H stretching bands, C—H antisymmetric, and symmetric stretching modes, as well as C—O bands, are detected in both fractions. The O—H band is very intense for the ASM $>$ 1 kDa (3362 cm^{-1}) and of medium intensity for the AIM (3292 cm^{-1}) fraction; the C—H bands are very intense for the AIM (2919 and 2850 cm^{-1}) and of medium to low intensity for the ASM $>$ 1 kDa (2921, 2851 cm^{-1}) fraction while the C—O bands are of medium intensities for both fractions (1071 and 1099 cm^{-1}).

Notably, the bands at 2921/2851 and 2919/2850 cm^{-1} for the ASM $>$ 1 kDa and AIM fractions, respectively, show the same relative shape and intensity as described for lipopolysaccharides (LPS).[65,66] These vibrations are attributed to the lipid nature of LPS and thus suggest the presence of lipids in these fractions. Because these bands are much more intense in the AIM than in the ASM, we propose that the dark colloidal suspension described above consists of lipids and/or lipopolysaccharides. Indeed, such suspension has already been suspected in some brachiopod shells,[67] while the presence of lipid has been identified in coral skeletons[68,69] and mollusk shells.[70,71]

Concerning the bands related to protein backbone, vibrational modes of nitrogen groups are assigned to N—H deformation in primary amides (1637 cm^{-1} in AIM, 1631 cm^{-1} in ASM $>$ 1 kDa) and N—H deformation in secondary amides (1541 cm^{-1} in AIM, 1433 cm^{-1} in ASM $>$ 1 kDa).[72] These bands show similar intensities in both fractions.

The FTIR spectra of the ASM $<$ 1 kDa fraction, composed of free PHNQs, are also presented for comparison, although no characteristic band of this fraction is clearly observed in the other two. It displays characteristic bands of PHNQs at 1719 and 1597 cm^{-1}, which are attributed to C═C stretching, C—O—H in-plane, and C═O stretching, respectively.[73] Bands at 1405 and 1278 cm^{-1} are also attributed to C—C and C—O stretching in PHNQs.[74] The presence of polysaccharide signatures at 2924 and 2852 cm^{-1} and of lipidic signature at 2924 cm^{-1} indicates that impurities may remain in this sample.

Overall, these assignments together with the respective band intensities indicate that proteins are present in both the ASM $>$ 1 kDa and AIM fractions, polysaccharides are more abundant in the ASM $>$ 1 kDa than in the AIM, while it is the opposite for lipids.

To separate the macromolecules associated with spinochrome A and to evidence some possible pigment-macromolecule interactions, all fractions were submitted to 15% Tricine-SDS PAGE (Figure 6C,D). Before staining, the gels are first

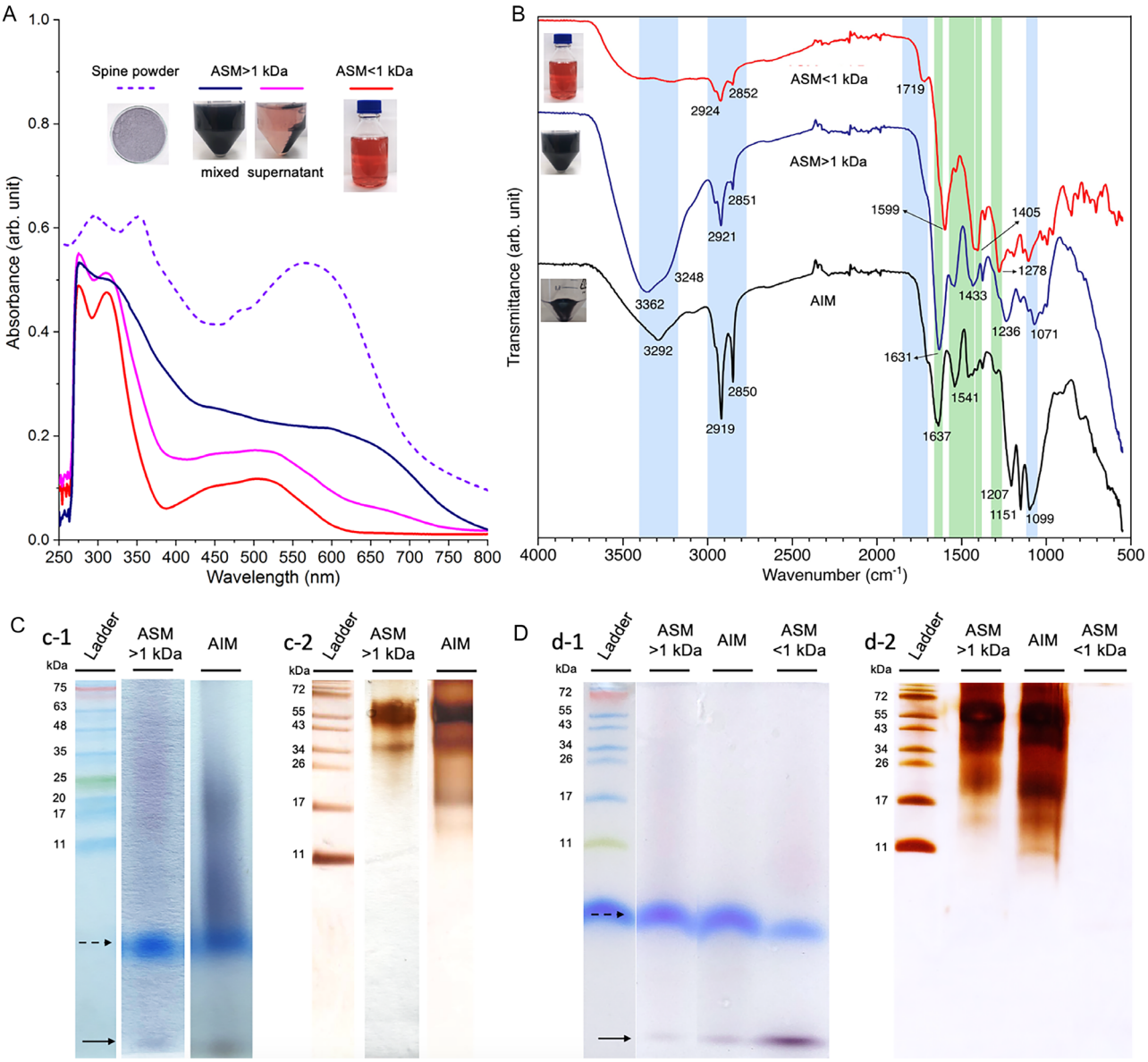

Figure 6. A) UV–visible spectroscopy of ASM < 1 kDa and ASM > 1 kDa compared to the DRS spectra of the powder, B) FTIR spectra of AIM, ASM < 1 kDa, and ASM > 1 kDa with vibrational modes usually associated to polysaccharides highlighted in blue and to proteins in green; and C,D) 15% Tricine-SDS-PAGE electrophoresis gels photographed before c-1, d-1) and after c-2, d-2) silver staining of the ASM > 1 kDa, ASM < 1 kDa and AIM fractions for two different extractions from purple spines. The dashed arrows point the migration front while the plain arrows show the free pigments.

photographed to report their different colorations (Figure 6c-1, d-1). The free pigment fraction (ASM < 1 kDa) shows the presence of an intense and discrete purple band at the bottom of the gel (below the blue migration front), attributed to the small free spinochrome A molecules (264 Da) (Figure 6d-1). This discrete purple band is also detected in the AIM and ASM > 1 kDa fractions, although it is less intense (Figure 6c-1). This result suggests the presence of spinochrome A in its free form or weakly bound to the macromolecules of the AIM and ASM > 1 kDa fractions. In addition, a purple smearing is observed along the lane for both the AIM and ASM > 1 kDa fractions. This purple smearing is particularly intense for the AIM from 20 kDa until the migration front and thus indicates a nonspecific complexation of spinochrome A with some macromolecules.

Silver staining is then used to identify most of the macromolecules and macromolecular complexes present in those fractions.[75–77] After staining (Figure 6c-2,d-2), the purple coloration disappears due to the decomplexation and subsequent diffusion of the pigment molecules out of the gel, likely caused by the use of TCA/methanol during the procedure. However, the previously observed purple smearing spatially correlates with some stained bands and a silver smearing. On one hand, the intense bands detected at around 20–25 kDa and 55 kDa for both the AIM and ASM > 1 kDa fractions suggest the presence of carbonic anhydrase and SM50 proteins, respectively. These proteins have been previously identified in the intracrystalline organic fraction of *P. lividus* test plates and are known to be involved in biomineral formation.[27,78] On the other hand, the silver

smearing indicates the presence of a complex mixture of macromolecules, potentially including polysaccharides.[79,80] The ASM $<$ 1 kDa fraction shows no band above the migration front, confirming the absence of macromolecules in this low molecular weight extract.

Altogether, these results show the isolation of intracrystalline pigment-macromolecule complexes in purple *P. lividus* sea urchin spines, whose pigment molecule is mainly spinochrome A, and the macromolecules include proteins, polysaccharides, and lipids.

2.5. Color Stability and Coloring Applications of Inorganic and Organic Materials

Natural dyes such as anthraquinones,[81] anthocyanins,[82] and naphthoquinones[83] derived from plants typically display halochromic properties, i.e., color changes according to pH. PHNQs extracted from *Mesocentrotus nudus* sea urchins were also shown to exhibit color changes from orange-red to yellow.[20] Here, we evidence color variations from orange-red to magenta, purple, and blue at pHs ranging from 4 to 12 for the entire colored organic fraction, as well as for the free PHNQ fraction of *P. lividus*. These different colors are mainly attributed to the successive deprotonation of the four hydroxyl groups of spinochrome A, the major PHNQ molecule (**Figure 7**A, Figure S4A, Supporting Information). Strikingly, the PHNQ-macromolecule complexes (AIM + ASM $>$ 1 kDa fractions) without the free PHNQ fraction, which was removed by ultrafiltration, display the same purple hue across the pH range tested (Figure 7A). This purple color stability with respect to pH is further confirmed during SDS-PAGE fixation, where the purple smearing attributed to the pigment-macromolecule complexes remains purple when pH decreases from 8 to 4, whereas the discrete purple band assigned to the

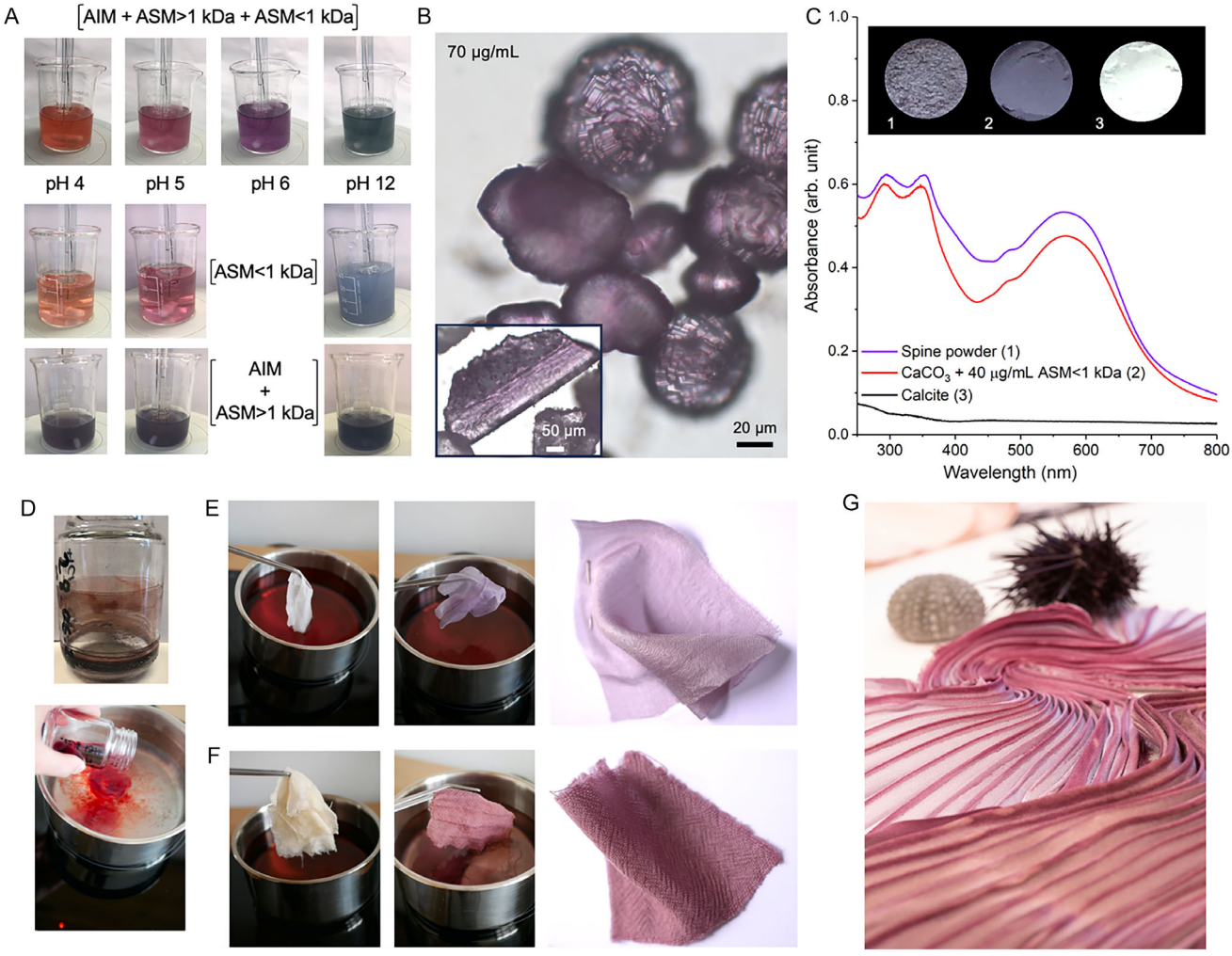

Figure 7. A) Photographs of color changes according to pH (from pH 4 to pH 12) of the total colored intracrystalline molecules, the free pigments (ASM $<$ 1 kDa) and the pigment-macromolecule complexes. B) Optical images of the spine powder (bottom left insert as compared to the $CaCO_3$ crystals formed by vapor diffusion in the presence of the total colored organic fraction (AIM + ASM $>$ 1 kDa + ASM $<$ 1 kDa, at 70 µg mL^{-1}) obtained after purple spine mineral dissolution with acetic acid. C) DRS spectra of a spine powder compared to the synthesized bio-based hybrid pigments obtained by direct precipitation in the presence of 40 µg/mL of ASM $<$ 1 kDa. D) Incorporation of the *P. lividus* free pigments (ASM $<$ 1 kDa) dissolved in ethanol into a water bath at 40 °C, E,F) photographs during the dyeing of a silk fabric shaded with acetic acid (top) and a wool fabric (bottom), and G) shibori dyeing of silk with *M. nudus* free pigments.

free pigments turns red at pH 4 (Figure S4B, Supporting Information). This color stability regarding pH is likely due to the stabilization of the deprotonation state of spinochrome A through its complexation with the macromolecules, thus contributing to the final purple color of the spines, once the pigment-macromolecule complexes are occluded within the calcite phase.

To test this hypothesis, the formation of calcite crystals was induced directly within the solution obtained immediately after mineral dissolution, thereby containing the three colored organic fractions and dissolved Ca^{2+} ions in acetic acid. This synthesis was adapted from the so-called vapor diffusion method classically used in biomineralization studies to study the effect of organics on crystal shapes.[26,64,84] Here, it involves the diffusion of $(NH_4)_2CO_3$ into the colored organic solution containing Ca^{2+} ions and results in the slow formation of $CaCO_3$ crystals recovered after four days (see Experimental Section). This method led to the formation of crystals with a purple hue very similar to that observed for powdered purple spines (Figure 7B, Figure S5A, Supporting Information), thus demonstrating the critical role of the entire colored organic fraction in contributing to the homogeneous purple color of the spines. We note that in the absence of the colored organic fraction, most crystals exhibit typical spherical shapes and granular surfaces of the vaterite phase, and only a few crystals display a rhombohedral shape characteristic of the calcite phase (Figure S5A, Supporting Information). In contrast, the presence of the colored molecules leads to the formation of larger crystals, also spherical but with faceted subunits resembling those observed for calcite crystals formed in acetic acid solution[85] (Figure S5A, Supporting Information). Although it is difficult to conclude on the nature of the $CaCO_3$ phase in this case, these results show that the presence of the colored molecules not only provides the purple color but also modifies crystal growth.

The effect of the free PHNQ fraction on $CaCO_3$ growth was further studied through the direct precipitation method.[86] This method consists of the fast addition of $CaCl_2$ solution into Na_2CO_3 and results in the precipitation of amorphous calcium carbonate, the mineral precursor described in vivo,[87,88] which further crystallizes in vitro into vaterite after a few minutes in solution, followed by the vaterite to calcite conversion after a few hours. Here, this synthesis was performed by adding the free PHNQ fraction (ASM $<$ 1 kDa) at 40 µg mL to the Na_2CO_3 solution before the addition of $CaCl_2$ (see Experimental Section). The nature of the different polymorphs was determined by X-ray diffraction (XRD) measurements after 48 h (Figure S5B, Supporting Information). In the absence of pigment, only calcite is formed, whereas in its presence, the vaterite phase persists, indicating the delay of the vaterite to calcite conversion. Free PHNQs therefore modify the kinetics of $CaCO_3$ formation as previously shown in the case of naphthazarin (5,8-dihydroxy-1,4-naphthoquinone),[89] an analog of PHNQs.

Concerning the color, the synthesized $CaCO_3$ powder shows a purple hue very similar to that of the spine powder, as confirmed by the UV–visible spectra (Figure 7C). As for naphthazarin,[89] which also changes in solution from red to purple at pH 8 (Figure S4A, Supporting Information), the purple color of the mineral powder is here attributed to pH variations occurring during the formation and crystallization of amorphous calcium carbonate, which likely control spinochrome A speciation. However, in this case, heterogeneously colored crystals are typically formed[89] as opposed to crystals obtained with the diffusion method in the presence of the entire colored organic fraction (Figure 7B).

Overall, these results demonstrate the crucial role of the entire colored organic fraction, in addition to the effect of pH, during $CaCO_3$ formation, which contributes to the final mass-color of biominerals. They also emphasize the significance of the developed methodology in isolating both free pigment and pigment-macromolecule complexes for investigating mechanisms of pigmentation and biomineralization.

Finally, we present the potential of the free pigment molecules for dyeing organic fibers. These pigments can be extracted from the skeletal parts of edible sea urchin species, such as *Paracentrotus lividus* and *Mesocentrotus nudus*, considered in this study. The production of sea urchins is estimated to be 75,000 tons/year.[7] The edible part, i.e., their gonads, represents 10 to 30% and the remaining skeletal elements (spines and test) approximately 30% of the entire sea urchin mass. Recent studies have demonstrated that sea urchin waste is a valuable resource for producing eco-sustainable products for a circular economy.[90,91] An additional source of waste could be the invasive sea urchin species from barrens such as *M. nudus*, which are free from gonads due to starvation after having destroyed entire kelp forests and cannot therefore be used for consumption, but need to be removed to restore the kelp forest ecosystem.[92,93]

Here, about 30 mg of free pigment molecules were extracted from *P. lividus* spines for dyeing mordanted silk and wool (see Experimental Section) (Figure 7D-F). Pigment extraction was also performed in higher quantity (15 g) from *M. nudus* obtained from food waste (2.5 kg). For this species, the main PHNQ molecule is reported to be spinochrome E.[11] In that case, we applied the pleating Shibori Japanese dyeing technique (see Experimental Section) (Figure 7G). Notably, both pigments produce intensely colored fabrics, despite the low dye-to-fabric ratio (0.01%), which highlights the high tinting strength of PHNQs. Moreover, different hues, ranging from purple to magenta, are obtained according to the nature of the fibers and the dyeing procedure, suggesting different deprotonation states of PHNQs and thus different complexations with silk and wool. Different purple hues and also orange colors can be obtained alternatively, depending on the extract and the dyeing procedure (Figure S6A and B, Supporting Information). To further demonstrate the potential of these dyes for use at higher scale levels, a few-meter textile artwork based on the shibori technique was successfully produced using the *M. nudus* pigment extract (Figure S7, Supporting Information).

Although these dyed fabrics show no apparent color changes after 3 years of storage (Figure S6C-H, Supporting Information), further systematic studies are needed to investigate their stability against light, heat, and washing cycles. In addition, while PHNQs are already considered for several biomedical applications, such as the treatment of nonhealing skin wounds,[94] safety

assessments are needed regarding their use in the textile industry, to confirm their usability in the textile color industry.

3. Conclusion

The tailored methodology reported in this work enables the valorization of colored seashell waste by extracting its pigment-macromolecule complexes, in addition to its small organic free pigments. It is based on an optimized cleaning of the soft tissues, a gentle dissolution of the mineral phase, and the recovery of all fractions, including the smallest in size. By applying this methodology to sea urchin skeleton waste, we identified the nature of these complexes, namely, PHNQ-macromolecule complexes. In addition, we demonstrated their color stability with respect to pH, as compared to free PHNQs, which change from red to purple at basic pH. Both color properties highlight, respectively, the crucial role of the pigment-macromolecule complexes and the pH at which biominerals are formed, in controlling the final color of biominerals. This conclusion is further supported by the bio-inspired synthesis of calcium carbonate in the presence of the extracted colored organic fraction, resulting in the formation of bio-inspired colored crystals. In addition to coloring inorganic materials, we successfully dye silk and wool fabrics, thereby illustrating the potential of the developed methodology for valorizing such a source of pigments in the color industry, which is actively turning to natural products.

4. Experimental Section

Sample Preparation

Paracentrotus lividus sea urchins were obtained from the biological station of Sorbonne University (Roscoff, France). *Mesocentrotus nudus* sea urchins were acquired from the Sakura-Maguro sea food company (https://sakura-maguro.com).

After dissection of the Aristotle's lantern, the coelomic fluid, the gonads, and the internal organs of each sea urchin are removed. Each carcass is soaked in 200 mL of 5 wt% sodium hypochlorite (NaClO) solution for 4 h to remove most of the organic tissues (podia, muscles, epidermis, etc.) until the spines detached from the tests. The spines are collected and further cleaned with 5 wt% NaClO for another 4 h under rotative agitation (Stuart rotator SB3, 15 rpm) and extensively rinsed with distilled water. These bleaching steps correspond to the first oxidative treatment of 8 h with 5 wt% NaClO. After drying under hood, spines of 1 cm long are selected and ground in an agate mortar to be sieved into $a < 200$ µm powder. The resulting powder is then subjected to a second oxidative treatment in 5 wt% NaClO solution (50 mL/per g of powder) for 4 h under rotative agitation to ensure the removal of intercrystalline organics. The NaClO concentration and exposure time were set by exposing freshly transversely fractured spines (3—5 mm long) to either 5% or 12% NaClO for 4 h, 12 h, or 48 h, and verifying the presence of residual organics. After centrifugation (MIKRO 220R Hettich centrifuge, 6000 rpm, 10 min, 25 °C), the NaClO solution is removed, the powder rinsed five times with Milli-Q water under rotative shaking for 30 min, once with methanol or alternatively ethanol for 5 min, and finally air-dried.[38] The concentration of the NaClO solutions refers to the available active chlorine and was measured by classic iodometric titration before every use, as it can vary over time.[95] Briefly, 1 mL of NaClO stock solution was mixed with 1 g of potassium iodide, and the volume was adjusted to 50 mL with Milli-Q water. The solution was acidified with 5 mL of glacial acetic acid and titrated with 0.1 M sodium thiosulfate. The completion of the titration was assured by adding 3 mL of 1% (m/v) starch when the analyte turned yellow. Three different batches of *P. lividus* powders are then produced, each comprising spines from 5 to 6 specimens.

Extraction and Isolation of the Intracrystalline Colored Organic Fraction

The intracrystalline organic molecules are extracted from purple spines by combining and adapting two established protocols for (i) the extraction of macromolecules from $CaCO_3$ skeletons;[26,29] and (ii) the isolation of pure $PHNQ_S$ from sea urchin biominerals.[11,22] After the oxidation treatment, 13.6 g of the < 200 µm powder is slowly dissolved under stirring at 4 °C with 470 mL of 1.75 M acetic acid solution added at a rate of 1.2 mL min^{-1} using a digital burette TITRONIC 300 until complete dissolution. The dissolution is performed at 4 °C to preserve the native structure of the proteins for further analysis using SDS-PAGE. However, higher-scale extraction for potential applications, such as dyeing, can be done at room temperature.[96]

The dissolved dark purple solution ($pH = 4.4$) is distributed into centrifuge tubes and centrifuged at 6000 rpm for 15 min at 4 °C. The pink supernatant containing the ASM is collected. The dark purple pellet containing the AIM is rinsed several times with 1.75 M acetic acid (≈40 mL) until the supernatant turns colorless, then one last time with Milli-Q water and freeze-dried. The supernatant from this rinsing step is added to the ASM fraction, yielding a final volume of 510 mL. The ASM fraction is further separated at 4 °C by ultrafiltration through a 1 kDa membrane under 2–4 bars using a 400 mL Millipore Amicon stirred cell. Therefore, two ASM fractions are obtained: ASM > 1 kDa and ASM < 1 kDa.

The separation of the AIM and the ASM can be skipped for applications that consider the entire colored organic fraction for dyeing applications.[96]

The ASM > 1 kDa fraction is then dialyzed at 4 °C against Milli-Q water using 0.5–1 kDa molecular weight cut-off dialysis tubes to remove ions from mineral dissolution. Several water changes are done until the volume within the dialysis tubes becomes constant. The dialyzed ASM is then concentrated by ultrafiltration through 1 kDa membrane and freeze-dried.

The ASM fraction < 1 kDa is further acidified to $pH = 2.0$ by adding concentrated (37 wt%) hydrochloric acid (HCl) and then partitioned between water and diethyl ether to isolate the free pigment molecules. The diethyl ether phase containing the PHNQs is collected, and another solvent extraction is performed involving an equal volume of 4 wt% sodium carbonate (Na_2CO_3) solution ($pH = 11$) and diethyl ether to further purify the PHNQ fraction from remaining lipids and oligopeptides. The Na_2CO_3 aqueous phase containing the PHNQs is collected, acidified back to $pH = 2.0$ with 6 M HCl, and partitioned again between water and diethyl ether. The ether extract is evaporated under a fume hood to yield a dark-red precipitate characteristic of PHNQ extracts, which is further freeze-dried.

Synthesis of the Colored Crystals

Vapor diffusion method: About 1 g of purple spine powder was sieved through 200 µm and dissolved with cold 1.75 M acetic acid

in a drop-wise manner under gentle agitation (around 35 mL g^{-1} of powder) in the fridge. The resulting solution was diluted four times with Milli-Q water, and the pH was adjusted from 4.4 to 5.8 with 4 M NaOH. Aliquots of 20 mL were transferred to 30 mL glass vials containing 1.5 × 1.5 cm glass slides at the bottom, and each was placed into a 1 L beaker along with one vial containing 2 g of $(NH_4)_2CO_3$. As a reference, another glass vial containing 20 mL of filtered (0.22 µm), freshly made 10 mM $CaCl_2$ (pH = 5.8) was prepared and purged with nitrogen for 5 h prior to use. All vials were sealed with Parafilm, and 5 holes were made on top of each. The beaker was sealed with Parafilm under the hood. The crystallization took place over 4 days at 20 °C, after which the glass slides were collected and rinsed with ethanol to remove any adsorbed particles and/or pigment. The slides were dried overnight in the oven at 37 °C. The final organic concentration of the AIM, ASM > 1 kDa, and ASM < 1 kDa was about 70 µg mL^{-1}.

Direct precipitation method: $CaCO_3$ precipitated in the presence of 40 µg mL of ASM < 1 kDa was synthesized over 48 h at room temperature using a Thermo Scientific Cimarec i Multipoint magnetic stirrer plate. Under continuous stirring at 300 rpm, 2 mL of 1 M $CaCl_2$ solution was added to the reaction medium (40 mM Na_2CO_3 and 40 µg mL^{-1} of ASM < 1 kDa) using a pipette within 8–10 s. The resulting precipitate was collected via Büchner filtration, rinsed with ethanol, and subsequently dried under vacuum in a vial for 30 min to remove residual moisture.

Textile Finishing

Dyeing procedure: Prior to dyeing, the silk and wool fabrics are mordanted with alum powder and cream of tartar. 30 mg of pigment previously extracted with 10% (v/v) acetic acid, 33% (m/v) citric acid, or 6 M HCl and recovered by solvent extraction is then diluted in 10 mL of ethanol and added to 2 L of water at 40 °C (pH 6). The temperature is progressively raised to 60 °C during continuous mixing of the solution for 15 min. The silk fabric is then introduced to the solution at 50 °C for 1 h, and the wool fabric at 40 °C for 1 h, while maintaining gentle agitation. Fabrics are finally washed with soap and rinsed in water twice to remove excess pigment. Silk fabrics can be additionally treated with 10% acetic acid for a shading step to tone the hue.

Pleating shibori procedure: The dyeing procedure described above is first applied on a large silk fabric before rolling and tying it around a cylinder. Additional ink, consisting of sea urchin pigments and aluminum sulfate, is applied to the fabric. Finally, the entire cylinder, with the tied fabric, is placed in an oven at 100 °C, allowing the fixation of the colorants through steaming. Thus, a three-dimensional form is created.

Optical Microscopy

Images were acquired on a Zeiss Axio Imager Vario using a 5-megapixels CMOS image sensor (Sony IMX 264 Exmor Pregius) with a pixel resolution of 3.45 µm and a size of 8.5 mm × 7.1 mm. The setup uses a microLED light source. Images have been captured in dark field mode as mosaics of pictures using a motorized stage.

Scanning Electron Microscopy (SEM) and Field Emission Gun (FEG)-SEM

SEM observations were performed with a Hitachi S-3400 microscope under an acceleration voltage of 10 kV. All samples were spin-coated with a 10 nm Pt layer to reduce surface charging. FEG-SEM observations were performed with a Hitachi SU-70 microscope under high vacuum and at an accelerating voltage of 2–5 kV.

UV–Visible Spectroscopy

The absorption spectra of the powdered spines and the extracted pigment in solution were recorded with a Cary 5000 Series UV–Vis–near-infrared (NIR) Spectrophotometer (Agilent Technologies). Single scans were performed within the range 200−800 nm (600 nm min^{-1} scan rate) either in absorbance mode (liquid samples) or in diffuse reflectance mode with an integrating sphere setup (solid samples). The $L^*a^*b^*$ values were obtained from the plotted powder spectra through the chromaticity diagram plugin on Origin 2024, considering the illuminant as D50 2° 1931, and converted online to sRGB values on Nix Color Sensor website (https://www.nixsensor.com/free-color-converter/).

Attenuated Total Reflectance (ATR)-FTIR

The vibrational spectra of the AIM, ASM > 1 kDa, and ASM < 1 kDa fractions were recorded using a Spectrum 400 FT-IR/FT-NIR Spectrometer (PerkinElmer) with a Universal ATR sampling accessory. Four scans per sample were performed from 550 to 4000 cm^{-1} on dry powder with a 4 cm^{-1} step resolution.

SDS-PAGE

The macromolecule profiles of the AIM, ASM > 1 kDa, and ASM < 1 kDa fractions were analyzed by discontinuous Tricine-SDS-PAGE to improve the resolution of low molecular weight components. The samples were dispersed in water and mixed with 2x Laemmli buffer (BioRad) containing 710 mM β-mercaptoethanol to reach a final protein concentration of 1 µg µL. All samples were homogenized and heated at 100 °C for 5 min to denature proteins, then centrifuged for approximately 15 s prior to gel loading. The 0.75- mm stacking and separating (15% polyacrylamide) gels, as well as the running anode and cathode buffers, were prepared according to Schägger and von Jagow (1987).[97] The gel was loaded with 20 µL of each sample as well as a protein standard ladder, and the run was performed at 100 V for sample stacking and 120 V for separation. The gels were directly stained with silver nitrate, as described by Morrissey (1981).[75]

HPLC MS

Liquid chromatography was performed in a LC-MS 2020 (SHIMADZU) through a Supelco Discovery HS C18 column (150 mm × 2.1 mm × 3 µm). The volume of sample injected was 5 µL, and the separation was conducted at a flow of 0.2 mL min^{-1}. The mobile phase consisted of acidified water (0.1% acetic acid) and acetonitrile, with an increasing proportion of acetonitrile to water from 10 to 100% (v/v). The UV detection was performed at 254 nm, and the mass detection of ions produced by electrospray ionization (ESI) scan (negative and positive) was done in the range of 100–800 m z^{-1}.

NMR

Liquid-state NMR experiments were conducted using a Bruker Avance III spectrometer equipped with a BBFO 5 mm probe, operating at 300.13 MHz for ^1H and 75.47 MHz for ^{13}C. The NMR spectra were recorded at a temperature of 25 °C in CD_2Cl_2 (stocked at 4 °C to limit water pollution). The chemical shifts of ^1H and ^{13}C were referenced to the solvent signals (5.32 ppm for $CHDCl_2$ and 53.84 ppm for CD_2Cl_2). ^1H-^{13}C heteronuclear multiple bonds correlation experiments[98] were

performed with a standard pulse program from Bruker's library (hmbcetgpl3nd) with no decoupling during acquisition and a three-fold low-pass J-filter to suppress one-bond correlations.

HR-MS

The identification of PHNQ molecules through HR-MS was performed using a LTQ Orbitrap XL spectrometer operating with ESI in negative mode with lockmass enabled. All lyophilized samples were solubilized in 100 μL methanol. m/z values were determined with a set resolution of 30,000. This allowed for high m/z accuracies, with typical errors below 2 ppm, helping to differentiate molecules of interest from isobaric compounds that could not be distinguished with lower resolution MS. At high m/z resolution, molecules are detected as isotopic patterns, that is, the distribution of the discrete isotopes constituting the molecule. The relative abundance of the different isotopes is given by the naturally occurring abundances of the different isotopes of their constitutive atoms.

XRD

HR-XRD measurements were conducted at the ID22 beamline (parameters: 35 keV, 1×1 mm^2 beamsize and $0.5-50°$ 2θ), ESRF Grenoble. XRD data were acquired on a rotating 0.7 mm capillary filled with sample powder. The beamline uses a 13-channel Si 111 multi-analyzer stage with a Dectris Eiger2 X 2M-W CdTe detector.[99,100] Data were normalized and rebinned into steps of 0.001° using the standard local software (id22sum). XRD data were plotted and analyzed using OriginPro software.

Acknowledgements

From Sorbonne University, David Montero is acknowledged for conducting FEG-SEM experiments, Mathilda Béarez and Camille Chareyron for helping with some extractions during their internships, Arturo Josué Alvarez Valverde for helping with some UV–visible measurements, and Guillaume Laurent for helpful discussions concerning color quantification. Lucile Chenais, a student at ENSCI—Les Ateliers, is also acknowledged for her help with pigment extraction during her internship. The authors are grateful to Cléo Verstrepen and Harumi Sugiura for organizing the collection of kitamurasaki uni, which resulted in the production of *M. nudus* waste. Hiroaki Kuno, a master of shibori pleating at Kunosen Factory (Arimatsu, Japan), is acknowledged for his help with the dyeing procedure. The authors acknowledge Andrew Fitch from the European Synchrotron Radiation Facility (ESRF) for support during beamtime and ESRF for allocating beamtime. This whole research has been mainly funded by the French National Research Agency (ANR, Grant ANR-20-CE08−0005). In addition, SEM-FEG microscope is funded by Sorbonne Université, CNRS and Région Ile de France, and the Federation of Chemistry and Materials of Paris-Center. Tony Jouanneau acknowledges Villa Kujoyama and Fondation Bettencourt for financial support.

Conflict of Interest

The authors declare no conflict of interest.

Author Contributions

Marie Alberic: conceptualization (lead); funding acquisition (lead); methodology (lead); supervision (lead); validation (lead); writing—original draft (lead); writing—review & editing: (lead)**; Claudio Ferreira**: investigation (lead); writing—original draft (lead); **Vaskar Sardhalia**: investigation (supporting); writing—review & editing (supporting); **Alshaba Kakar**: investigation (supporting); **Romain Descamps**: investigation: (supporting); methodology (supporting); **Lucrèce Matheron**: investigation (supporting); methodology (supporting); writing—review & editing (supporting); **François Ribot**: investigation: (supporting); writing—review & editing (supporting); **Alexandre Disser**: investigation (supporting); writing—review & editing (supporting); **Tony Jouanneau**: investigation: (supporting); **Elena Vasileva**: conceptualization (supporting); investigation (supporting); validation (supporting); writing—review & editing (supporting); **Natalia Mishchenko**: methodology (supporting); validation (supporting); writing—review & editing (supporting); **Nadine Nassif**: conceptualization (supporting); methodology (supporting); supervision (supporting); validation (supporting); writing—review & editing: (supporting); **Frederic Marin**: conceptualization (supporting); investigation (supporting); methodology (supporting); validation (supporting); writing—review & editing (supporting).

Data Availability Statement

The data that support the findings of this study are available from the corresponding author upon reasonable request.

Keywords: biomineral pigmentation · color stability · pigment-macromolecule complexes · textile finishing

[1] M. A. Manavi, M. Salehi, R. M. Jafari, A. R. Dehpour, *Arch. Pharm.* **2024**, *357*, https://doi.org/10.1002/ardp.202400532.
[2] L. Mabuza, N. Sonnenberg, N. Marx-Pienaar, *Resources. Conservation & Recycling Advances* **2023**, *18*, 200146.
[3] M. D. Stanescu, *Environ. Sci. Pollut. Res.* **2021**, *28*, 14253.
[4] W. M. Bandaranayake, *Nat. Prod. Rep.* **2006**, *23*, 223.
[5] S. T. Williams, *Biol. Rev.* **2017**, *92*, 1039.
[6] J. P. Morris, T. Backeljau, G. Chapelle, *Rev. Aquac.* **2019**, *11*, 42.
[7] G. Stefánsson, H. Kristinsson, C. H. Nikoline Ziemer, P. James, **2017**, https://doi.org/10.13140/RG.2.2.12657.99683.
[8] N. Yan, X. Chen, *Nature* **2015**, *524*, 155.
[9] Y. Hou, E. A. Vasileva, A. Carne, M. McConnell, A. E.-D. A. Bekhit, N. P. Mishchenko, *Rsc Adv.* **2018**, *8*, 32637.
[10] A. N. Shikov, O. N. Pozharitskaya, A. S. Krishtopina, V. G. Makarov, *Phytochem. Rev.* **2018**, *17*, 509.
[11] E. A. Vasileva, N. P. Mishchenko, V. T. T. Tran, H. M. N. Vo, S. A. Fedoreyev, *Mar. Drugs* **2021**, *19*, 21.
[12] L. Brasseur, E. Hennebert, L. Fievez, G. Caulier, F. Bureau, L. Tafforeau, P. Flammang, P. Gerbaux, I. Eeckhaut, *Mar. Drugs* **2017**, *15*, 179.
[13] C. J. Coates, C. McCulloch, J. Betts, T. Whalley, *J. Innate Immun.* **2018**, *10*, 119.
[14] A. V. Lebedev, E. L. Levitskaya, E. V. Tikhonova, M. V. Ivanova, *Biochemistry (Moscow)* **2001**, *66*, 885.
[15] C. Powell, A. D. Hughes, M. S. Kelly, S. Conner, G. J. McDougall, *LWT—Food Sci. Technol.* **2014**, *59*, 455.
[16] D.-Y. Zhou, L. Qin, B.-W. Zhu, X.-D. Wang, H. Tan, J.-F. Yang, D.-M. Li, X.-P. Dong, H.-T. Wu, L.-M. Sun, X.-L. Li, Y. Murata, *Food Chem.* **2011**, *129*, 1591.

[17] D. L. Fox, T. S. Hopkins, *Physiology of Echinodermata: A Collective Effort by a Group of Experts*, Boolootian R.A., Interscience Publishers, New York **1966**, 77–300.
[18] K. M. Towe, *Paleobiology* **1990**, *16*, 521.
[19] F. H. Wilt, *Zoolog. Sci.* **2002**, *19*, 253.
[20] D. Zhou, B. Zhu, X. Wang, L. Qin, D. Li, L. Miao, Y. Murata, *Int. J. Food Sci. Technol.* **2012**, *47*, 1479.
[21] L. Brasseur, M. Demeyer, C. Decroo, G. Caulier, P. Flammang, P. Gerbaux, I. Eeckhaut, *R. Soc. Open Sci.* **2018**, *5*, 171213.
[22] T. W. Goodwin, S. Srisukh, *Biochem. J.* **1950**, *47*, 69.
[23] S. Marzorati, G. Martinelli, M. Sugni, L. Verotta, *Front. Nutr.* **2021**, *8*, https://doi.org/10.3389/fnut.2021.730747.
[24] M. Fay, B. M. Hendrix, *J. Biol. Chem.* **1931**, *93*, 667.
[25] F. Marin, R. Amons, N. Guichard, M. Stigter, A. Hecker, G. Luquet, P. Layrolle, G. Alcaraz, C. Riondet, P. Westbroek, *J. Biol. Chem.* **2005**, *280*, 33895.
[26] J. M. Kanold, N. Guichard, F. Immel, L. Plasseraud, M. Corneillat, G. Alcaraz, F. Brümmer, F. Marin, *FEBS J.* **2015**, *282*, 1891.
[27] K. Karakostis, I. Zanella-Cléon, F. Immel, N. Guichard, P. Dru, T. Lepage, L. Plasseraud, V. Matranga, F. Marin, *J. Proteomics* **2016**, *136*, 133.
[28] B. Marie, C. Joubert, A. Tayalé, I. Zanella-Cléon, C. Belliard, D. Piquemal, N. Cochennec-Laureau, F. Marin, Y. Gueguen, C. Montagnani, *Proc. Natl. Acad. Sci.U.S.A.* **2012**, *109*, 20986.
[29] J. Sakalauskaite, L. Plasseraud, J. Thomas, M. Albéric, M. Thoury, J. Perrin, F. Jamme, C. Broussard, B. Demarchi, F. Marin, *J. Struct. Biol.* **2020**, *211*, 107497.
[30] M. Cianci, P. J. Rizkallah, A. Olczak, J. Raftery, N. E. Chayen, P. F. Zagalsky, J. R. Helliwell, *Proc. Natl. Acad. Sci.* **2002**, *99*, 9795.
[31] A. Comfort, *Biol. Rev.* **1951**, *26*, 285.
[32] K. Mann, D. Jackson, *BMC Genomics* **2014**, *15*, 249.
[33] M. Cusack, G. Curry, H. Clegg, G. Abbott, *Comp. Biochem. Physiol. B: Comp. Biochem.* **1992**, *102*, 93.
[34] B. M. Heatfield, *J. Morphol.* **1971**, *134*, 57.
[35] P. Gorzelak, A. Dery, P. Dubois, J. Stolarski, *Front. Zool.* **2017**, *14*, https://doi.org/10.1186/s12983-017-0227-8.
[36] S. Weiner, *J. Exp. Zool.* **1985**, *234*, 7.
[37] S. Weiner, *Calcif. Tissue Int.* **1979**, *29*, 163.
[38] K. E. H. Penkman, D. S. Kaufman, D. Maddy, M. J. Collins, *Quat. Geochronol.* **2008**, *3*, 2.
[39] M. Albéric, E. N. Caspi, M. Bennet, W. Ajili, N. Nassif, T. Azaïs, A. Berner, P. Fratzl, E. Zolotoyabko, L. Bertinetti, Y. Politi, *Cryst. Growth Des.* **2018**, *18*, 2189.
[40] F. Marin, L. Pereira, P. Westbroek, *Protein Expr. Purif.* **2001**, *23*, 175.
[41] J. S. Pearse, V. B. Pearse, A. Zool, *Am. Zool.* **1975**, *15*, 731.
[42] S. Seesanong, C. Seangarun, B. Boonchom, S. Phutphat, P. Rungrojchaipon, N. Montri, S. Thompho, W. Boonmee, N. Laohavisuti, *ACS Omega* **2023**, *8*, 27044.
[43] J. Aizenberg, G. Lambert, S. Weiner, L. Addadi, *J. Am. Chem. Soc.* **2002**, *124*, 32.
[44] L. Ameye, G. De Becker, C. Killian, F. Wilt, R. Kemps, S. Kuypers, P. Dubois, *J. Struct. Biol.* **2001**, *134*, 56.
[45] P. Dubois, M. Jangoux, Proceedings of the Fifth International Echinoderm Conference, Balkema, Rotterdam, **1985**, 507–512.
[46] A. I. Scott, *Interpretation of the Ultraviolet Spectra of Natural Products*, Elsevier, Oxford **1964**.
[47] I. Singh, R. T. Ogata, R. E. Moore, C. W. J. Chang, P. J. Scheuer, *Tetrahedron* **1968**, *24*, 6053.
[48] W. Mokrzycki, M. Tatol,*Machine Graphics and Vision*, **2011**.
[49] A. Berman, J. Hanson, L. Leiserowitz, T. F. Koetzle, S. Weiner, L. Addadi, *Science* **1993**, *259*, 776.
[50] M. A. Crenshaw, *Biomineralisation* **1972**, *6*, 6.
[51] F. Marin, I. Bundeleva, T. Takeuchi, F. Immel, D. Medakovic, *J. Struct. Biol.* **2016**, *196*, 98.
[52] S. Weiner, L. Hood, *Science* **1975**, *190*, 987.
[53] L. Brasseur, G. Caulier, P. Flammang, P. Gerbaux, I. Eeckhaut, *Nat. Prod. Commun.* **2018**, *13*, 1934578X1801301.
[54] A. Verdes, W. Cho, M. Hossain, P. L. R. Brennan, D. Hanley, T. Grim, M. E. Hauber, M. Holford, *PLOS ONE* **2015**, *10*, e0143545.
[55] F. Marin, G. Luquet, in *Handbook of Biomineralization*, E. Bäuerlein, Wiley, Weinheim, Germany **2007**, 273–290.
[56] A. P. Wheeler, K. W. Rusenko, J. W. George, C. S. Sikes, *Comp. Biochem. Physiol. B: Comp. Biochem.* **1987**, *87*, 953.
[57] N. P. Mischenko, S. A. Fedoreyev, N. D. Pokhilo, V. P. Anufriev, V. A. Denisenko, V. P. Glazunov, *J. Nat. Prod.* **2005**, *68*, 1390.
[58] M. Roncoroni, G. Martinelli, S. Farris, S. Marzorati, M. Sugni, *Mar. Drugs* **2024**, *22*, 163.
[59] F. Louise, F. Benard, *Bull. Soc. Zool. Fr.* **1993**, *118*, 405.
[60] E. Lederer, *Biochim. Biophys. Acta* **1952**, *9*, 92.
[61] E. A. Vasileva, N. P. Mishchenko, P. A. Zadorozhny, S. A. Fedoreyev, *Nat. Prod. Commun.* **2016**, *11*, 1934578X1601100631.
[62] N. P. Mishchenko, E. A. Vasileva, A. V. Gerasimenko, V. P. Grigorchuk, P. S. Dmitrenok, S. A. Fedoreyev, *Molecules* **2020**, *25*, 4778.
[63] S. Albeck, S. Weiner, L. Addadi, *Chem. - Eur. J.* **1996**, *2*, 278.
[64] S. Albeck, J. Aizenberg, L. Addadi, S. Weiner, *J. Am. Chem. Soc.* **1993**, *115*, 11691.
[65] S. J. Parikh, J. Chorover, *Colloids Surf., B* **2008**, *62*, 188.
[66] M. Hassan, I. Ilev, *Rev. Sci. Instrum.* **2014**, *85*, https://doi.org/10.1063/1.4897247.
[67] G. C. Curry, M. Cusack, D. Walton, K. Endo, H. Clegg, G. Abbott, H. Armstrong, *Phil. Trans. R. Soc. Lond. B.* **1991**, *333*, 359.
[68] Y. Isa, M. Okazaki, *Comp. Biochem. Physiol. B: Comp. Biochem.* **1987**, *87*, 507.
[69] M. Reggi, S. Fermani, C. Samorì, F. Gizzi, F. Prada, Z. Dubinsky, S. Goffredo, G. Falini, *CrystEngComm* **2016**, *18*, 8829.
[70] E. A. Cobabe, L. M. Pratt, *Geochim. Cosmochim. Acta* **1995**, *59*, 87.
[71] B. Farre, Y. Dauphin, *Comp. Biochem. Physiol. B: Biochem. Mol. Biol.*, **2009**, *152*, 103.
[72] H. F. Shurvell, *Handbook of Vibrational Spectroscopy*, Chalmers J.M., Wiley, New Jersey, USA **2006**, 1783–1816.
[73] V. P. Glazunov, D. V. Berdyshev, *J. Appl. Spectrosc.* **2014**, *81*, 553.
[74] M. Z. Tabrizi, S. F. Tayyari, F. Tayyari, M. Behforouz, *Spectrochim. Acta, Part A* **2004**, *60*, 111.
[75] J. H. Morrissey, *Anal. Biochem.* **1981**, *117*, 307.
[76] H. Blum, H. Beier, H. J. Gross, *Electrophoresis* **1987**, *8*, 93.
[77] D. C. Blake, R. G. Russell, *Infect. Immun.* **1993**, *61*, 5384.
[78] K. P. Campbell, D. H. MacLennan, A. O. Jorgensen, *J. Biol. Chem.* **1983**, *258*, 11267.
[79] D. Gaspard, F. Marin, N. Guichard, S. Morel, G. Alcaraz, G. Luquet, *Earth Environ. Sci. Trans. R. Soc. Edinburgh* **2007**, *98*, 415.
[80] F. Marin, F. Immel, N. Trinkler, D. Gaspard, F. Marin, F. Brümmer, A. Checa, G. Furtos, I. G. Lesci, L. Šiller, *Biomineralization: From Fundamentals to Biomaterials & Environmental Issues*, F.Marin, F. Brümmer, A. Checa, G. Furtos, I. G. Lesci, L. Šiller, Trans Tech Publications Ltd., Switzerland **2015**, 215–221.
[81] T. H. L. Tran, B. Rigaud, M. Jaber, R. Berraud-Pache, *Dyes Pigm.* **2024**, *228*, 112242.
[82] M. Rusishvili, L. Grisanti, S. Laporte, M. Micciarelli, M. Rosa, R. J. Robbins, T. Collins, A. Magistrato, S. Baroni, *Phys. Chem. Chem. Phys.* **2019**, *21*, 8757.
[83] E. J. Land, T. Mukherjee, A. J. Swallow, J. M. Bruce, *J. Chem. Soc., Faraday Trans. 1* **1983**, *79*, 391.
[84] N. Nassif, F. Martineau, O. Syzgantseva, F. Gobeaux, M. Willinger, T. Coradin, S. Cassaignon, T. Azaïs, M. M. Giraud-Guille, *Chem. Mater.* **2010**, *22*, 3653.
[85] G. E. Henderson, B. J. Murray, K. M. McGrath, *J. Cryst. Growth* **2008**, *310*, 4190.
[86] Z. Zou, L. Bertinetti, Y. Politi, A. C. S. Jensen, S. Weiner, L. Addadi, P. Fratzl, W. J. E. M. Habraken, *Chem. Mater.* **2015**, *27*, 4237.
[87] M. Albéric, C. A. Stifler, Z. Zou, C.-Y. Sun, C. E. Killian, S. Valencia, M.-A. Mawass, L. Bertinetti, P. U. P. A. Gilbert, Y. Politi, *J. Struct. Biol.:X* **2019**, *1*, 100004.
[88] Y. Politi, T. Arad, E. Klein, S. Weiner, L. Addadi, *Science* **2004**, *306*, 1161.
[89] V. Sardhalia, C. dos Reis Ferreira, G. Laurent, M. Selmane, A. Vallée, M. Fregnaux, D. Talbot, X. Li, M. de Frutos, A. Fitch, I. Polishchuk, B. Pokroy, C. Schmitt, S. Amini, P. Fratzl, T. Azaïs, N. Nassif, **2025**, https://doi.org/10.21203/rs.3.rs-5965086/v1.
[90] F. Zilia, J. Bacenetti, M. Sugni, A. Matarazzo, L. Orsi, *Sustainability* **2021**, *13*, 5427.
[91] F. Zilia, L. Orsi, M. Costantini, D. E. A. Tedesco, M. Sugni, *Clean. Environ. Syst.* **2023**, *8*, 100108.
[92] K. Filbee-Dexter, R. Scheibling, *Mar. Ecol. Prog. Ser.* **2014**, *495*, 1.
[93] Y. Agatsuma, T. Abe, E. Inomata, S. Takagi, K. Tanaka, M. Hirotsune, K. Maeda, M. Aoki, *Mar. Ecol. Prog. Ser.* **2024**, *748*, 17.
[94] L. Melotti, A. Venerando, G. Zivelonghi, A. Carolo, S. Marzorati, G. Martinelli, M. Sugni, L. Maccatrozzo, M. Patruno, *Antioxidants* **2023**, *12*, 1730.

[95] W. C. Lipps, E. B. Braun-Howland, T. E. Baxter, in *Water Environment Federation, Eds., in Standard Methods for the Examination of Water and Wastewater*, American Public Health Association, American Water Works Association, American Public Health Association, Washington, **2023**, 347–352.
[96] M. Albéric, F. Marin, C. R. Ferreira, *Novel Form of Sea Urchin Pigments, and Uses Thereof*, **2023**, WO2025062069.
[97] H. Schägger, G. von Jagow, *Anal. Biochem.* **1987**, *166*, 368.
[98] D. O. Cicero, G. Barbato, R. Bazzo, *J. Magn. Reson.* **2001**, *148*, 209.
[99] T. Donath, D.Šišak Jung, M. Burian, V. Radicci, P. Zambon, A. N. Fitch, C. Dejoie, B. Zhang, M. Ruat, M. Hanfland, C. M. Kewish, G. A. Van Riessen, D. Naumenko, H. Amenitsch, G. Bourenkov, G. Bricogne, A. Chari, C. Schulze-Briese, *J. Synchrotron Radiat.* **2023**, *30*, 723.
[100] A. Fitch, C. Dejoie, E. Covacci, G. Confalonieri, O. Grendal, L. Claustre, P. Guillou, J. Kieffer, W. De Nolf, S. Petitdemange, M. Ruat, Y. Watier, *J. Synchrotron Radiat.* **2023**, *30*, 1003.

Manuscript received: June 13, 2025
Revised manuscript received: September 12, 2025
Version of record online: